

Anomaly-Aware YOLO: A Frugal yet Robust Approach to Infrared Small Target Detection

Alina Ciocarlan^{a,*}, Sylvie Le Hégarat-Mascle^b, Sidonie Lefebvre^c

^aFrench Ministerial Agency for Defense AI (AMIAD), 91120 Palaiseau, France

^bSATIE, Paris-Saclay University, 91405 Orsay, France

^cDOTA & LMA2S, ONERA, Paris-Saclay University, F-91123 Palaiseau, France

Abstract

Infrared Small Target Detection (IRSTD) is a challenging task in defense applications, where complex backgrounds and tiny target sizes often result in numerous false alarms using conventional object detectors. To overcome this limitation, we propose Anomaly-Aware YOLO (AA-YOLO), which integrates a statistical anomaly detection test into its detection head. By treating small targets as *unexpected* patterns against the background, AA-YOLO effectively controls the false alarm rate. Our approach not only achieves competitive performance on several ISTD benchmarks, but also demonstrates remarkable robustness in scenarios with limited training data, noise, and domain shifts. Furthermore, since only the detection head is modified, our design is highly generic and has been successfully applied across various YOLO backbones, including lightweight models. It also provides promising results when integrated into an instance segmentation YOLO. This versatility makes AA-YOLO an attractive solution for real-world deployments where resources are constrained. The code will be publicly released.

Keywords:

YOLO, anomaly detection, infrared small target, statistical testing

1. Introduction

InfraRed Small Target Detection (IRSTD) is a highly challenging yet critical task in defense, characterized by tiny target sizes, complex backgrounds, and difficult learning conditions. Deep learning-based ISTD methods have been proposed to tackle these challenges, achieving State-Of-The-Art (SOTA) performance. These approaches leverage techniques such as dense nested architectures [1] or attention mechanisms [2, 3] to mitigate information loss on small targets and reduce confusion with background elements. However, current SOTA ISTD methods face limitations due to their reliance on segmentation networks. One major issue is that their evaluation is heavily influenced by subjective annotations, as illustrated in Figure 1. Specifically, annotators may label entire vehicles or highlight the most salient regions with high InfraRed (IR) responses, leading to contradictory training signals. These inconsistencies can significantly affect both the training process and the pixel-level evaluation metrics. Furthermore, segmentation-based methods often suffer from i) object fragmentation when binarizing feature maps, and ii) adjacency issues, where two nearby targets are mistakenly detected as a single object. These issues affect counting accuracy, especially in critical domains like civil security.

Object detection algorithms such as YOLO [4] help mitigate this risk by explicitly localizing objects through bounding box regression, with faster inference times. Although annotation



Figure 1: Illustration of the annotation subjectivity in ISTD. The top-right corners show in blue the annotation masks provided by [8] for the SIRST dataset.

subjectivity has less impact when switching from pixel-level to object-level annotations, it remains non-negligible for small objects. Indeed, [5] highlight that even minor localization errors can severely impact Intersection over Union (IoU) metrics for small objects, impairing both training and evaluation for YOLO networks. Recent approaches [6, 7] address these issues by reducing the influence of IoU loss on small objects and proposing alternative loss functions. While effective, SOTA methods often result in complex, task-specific models that may not adapt well to real-world scenarios with limited resources.

In this paper, we advocate for a complementary direction: **detecting small IR targets as statistical anomalies with respect to the background**. By treating small targets as *unexpected* patterns against the background, we adopt a statistical hypothesis testing framework where the background distribution is modeled as the null hypothesis. Importantly, this test is performed in latent space and requires minimal assumptions on background structure. We rely on a pragmatic exponential modeling, grounded in the maximum entropy principle [9], to de-

*Corresponding author

Email address: alina.ciocarlan@polytechnique.edu (Alina Ciocarlan)

rive an interpretable objectness score that tightly controls false alarms. Unlike traditional object detectors, our approach explicitly models the *unexpectedness* of small objects in the latent space, enabling both i) effective anomaly identification and ii) explicit control of the false alarms. Our method achieves strong performance under different types of frugality:

- *Data frugality*: our method retains at least 90% of the full-performance SIRST dataset [8], even when trained with only 10% of the data.
- *Computational frugality*: even when using lighter networks, our approach is competitive with SOTA, making it suitable for deployment on resource-constrained devices.
- *Generic design*: our method is easy to implement, requiring only a simple modification of the detection head. This makes our approach highly adaptable and user-friendly.

For these reasons, our Anomaly-Aware YOLO (AA-YOLO) is a compelling solution for real-world applications where computational and data resources are limited. Our main contributions can be summarized as follows:

1. We propose a simple yet effective YOLO detection head called the Anomaly-Aware Detection Head (AADH) that integrates statistical anomaly testing to improve IRSTD. Our method provides an anomaly-informed objectness score that empirically suppresses background.
2. By adding our AADH module to several conventional YOLO backbones, especially lightweight ones, we close the performance gap with SOTA methods. Notably, AA-YOLOv7t achieves SOTA results on famous IRSTD benchmarks while having six times fewer training parameters than EFLNet. It also gives promising results when integrated into an instance segmentation YOLO.
3. AADH significantly improves robustness in frugal settings, transfer learning, inference on noisy data, and operational contexts.
4. Lastly, our AADH facilitates the choice of a detection threshold by constraining all background values to zero.

2. Related works

2.1. IRSTD methods

The specificity of IRSTD lies in the extremely small size and low contrast ratio of the targets, making them particularly difficult to detect against complex backgrounds. Researchers have developed various deep learning-based strategies that surpass traditional methods for IRSTD. These methods fall into two main categories.

Segmentation methods. Segmentation networks are particularly popular among IRSTD methods due to their inherent ability to extract fine-grained features. To further enhance small target detection and reduce confusion with background clutter, [10, 2, 3] introduce attention mechanisms in their backbones.

Specifically, RDIAN [11] integrates convolution-based multidirectional guided attention mechanisms to enhance small target features in deep layers, while SCTransNet and DATransNet rely on the recent Transformer backbones to improve global scene understanding. An important issue with deep neural networks is their pooling layers, which degrade the amount of information for small targets. To mitigate this, [1] introduce DNANet, a dense-nested U-shaped backbone that leads to great performance on widely used IRSTD benchmarks. Other approaches attempt to resolve the limitations of IoU-based metrics for small objects by introducing alternative loss functions. For instance, MSHNet [12] proposes a location- and scale-sensitive loss, which significantly improves performance when combined with a simple U-Net architecture.

However, these methods are not robust to fragmentation issues that arise when binarizing segmentation maps, which can distort object counts. Additionally, they are prone to adjacency errors, where two adjacent objects are incorrectly merged. This leads to the exploration of object detectors with bounding box regression for IRSTD.

Object detection methods. Object detection involves detecting objects of interest within an image and identifying their locations with bounding boxes. Several deep learning approaches have been proposed for this task, including the popular YOLO framework [4]. While YOLO detectors achieve great performance in various applications with low inference time, they struggle to detect small objects due to two key factors: (1) class imbalance between target and background samples; and (2) low tolerance to bounding box localization errors for small objects, as even minor offsets can cause large drops in IoU. To address these issues, dedicated loss functions [6] have been introduced to increase the relative importance of minority samples. Additionally, [7] propose to reduce the weight of the IoU metric in the loss for small objects through their Scale Dynamic (SD) loss. The authors of EFLNet [6] go even further by replacing IoU-based loss with the Normalized Wasserstein Distance, as proposed in [13]. EFLNet’s performance on IRSTD benchmarks is particularly noteworthy, surpassing SOTA segmentation-based methods and setting a new performance standard for YOLO-based networks for IRSTD.

It is worth noting that existing papers often only partially address the various aspects of frugality. While some lightweight detectors for IRSTD have been proposed [14, 15], their robustness in frugal settings is rarely evaluated. Our paper aims to bridge these gaps by introducing a simple, resource-efficient, yet versatile approach that not only achieves SOTA performance for IRSTD but also demonstrates robustness.

2.2. Anomaly detection

The small size, lack of structure and scarcity of the targets make them natural candidates for anomaly detection. Indeed, this task aims to identify rare events that deviate from the standard and for which only limited samples are available. According to [16], these methods can fall into four main categories: distance-based methods (e.g., isolation forest or k-nearest

neighbors), reconstruction-based methods, one-class classification methods, and probabilistic methods. Reconstruction-based methods detect anomalies as inputs that are challenging to reconstruct accurately [17, 18]. One-class classification methods, such as Deep SVDD [19], train solely on normal samples and learn a compact representation or boundary around them, flagging outliers as anomalies. Probabilistic methods instead aim to model the probability density function of the normal data, identifying anomalies as samples with low likelihood. A notable example is the Reed-Xiaoli algorithm widely used in hyperspectral anomaly detection [20]. Note that hypothesis testing also falls into this category. Despite its potential, the integration of anomaly detection into end-to-end supervised learning frameworks for IRSTD remains limited. For example, [21] treat small targets as “noise” in an infrared background, reframing the detection problem to a denoising task. Similarly, [22] model the background in an unsupervised manner using VAEs and then applies a supervised detection algorithm to the resulting difference image. While promising, we argue that explicitly integrating the notion of *anomaly* within a supervised detection pipeline to guide feature extraction could improve robustness and accuracy, particularly in challenging scenarios where traditional methods often fail.

3. Proposed method

Our objective is to improve small target detection, especially under challenging conditions, by introducing an anomaly-based prior into a YOLO-type network. To this end, we train the network not to estimate the decision boundaries between target and non-target data points, as is conventionally done in detection networks, but rather to identify deviations from the background model. This is done by constraining the feature extraction using a probabilistic anomaly detection method. Integrating this statistical criterion into the training loop of a YOLO network ensures that, after convergence, only the targets violate the learned background model.

3.1. Formulation of the statistical anomaly testing

Our contribution consists in re-estimating the objectness scores predicted by the YOLO detection head for each bounding box using multiple statistical tests rejecting the null hypothesis H_0 . To this end, we consider the N voxels from the final feature map of dimension $H \times W \times C$, where H , W and C are the height, width and number of channels of the feature map, respectively. Each voxel $v_k \in \mathbb{R}^{1 \times 1 \times C}$ is represented by a C -dimensional random variable $X_k = (X_{k,1}, \dots, X_{k,C})$, where $X_{k,1}, \dots, X_{k,C}$ are assumed to be independent and identically distributed (i.i.d.). Note that the i.i.d. assumption across feature channels is a simplification and does not strictly reflect the dependencies learned by CNNs. However, in our context, this assumption does not aim to describe the exact generative process of feature activations, but to provide a tractable and interpretable null hypothesis for anomaly detection. According to the null hypothesis H_0 (to be rejected), a given voxel belongs to the background class. Our focus here is on controlling the Type

I error rate, i.e. the probability of rejecting H_0 when it is actually true. When performing multiple hypothesis tests, this can be framed as controlling the Family-Wise Error Rate (FWER). Let $\theta \in \mathbb{R}^*$ be the rejection threshold, F the testing function, and μ a measure. The FWER at confidence level $\alpha \in \mathbb{R}^*$ is defined as:

$$\mathbb{P}_{H_0}(\exists k \in \llbracket 1, N \rrbracket, F(\mu(X_k)) < \theta) < \alpha. \quad (1)$$

To compute the FWER, we define F as the p-value function. Given an observation x_k , the p-value is expressed as:

$$F(\mu(x_k)) = \mathbb{P}_{H_0}(\mu(X_k) \geq \mu(x_k)). \quad (2)$$

Let us now focus on our problem to explicitly define H_0 and F . First, note that our objective is not to perfectly fit the latent distribution of background voxels, but to select a plausible null hypothesis enabling effective anomaly discrimination, which is sufficient for our operational goals. Modeling IR background distributions can be challenging due to dynamic textures. However, our anomaly test operates in latent space, where background voxel features tend to cluster near zero after the ReLU activation, regardless of input image complexity. In this latent space, assuming an exponential distribution is well justified since it is the maximum entropy distribution among non-negative variables with fixed mean. Thus, according to the principle of maximum entropy [9], this makes it the minimally biased choice, introducing only the known constraints (here, non-negativity and empirical mean). Note that this assumption is pragmatically validated, as alternative hypotheses (e.g., Gaussian) lead to inferior detection performance (see our ablation study in Section 5), suggesting that the exponential assumption better aligns with the structure of the latent features. We therefore define the null hypothesis H_0 as assuming that each voxel follows a C -dimensional exponential distribution \mathcal{E} with parameter $\Lambda = [\lambda_1, \dots, \lambda_C]^T$.

Then, two aggregated measures μ admitting closed-form distributions under the exponential hypothesis can be considered:

1. $\mu_1(X_k) = \min\{X_{k,1}, \dots, X_{k,C}\}$ – In this case, the minimum of the channel values follows an exponential distribution with parameter $\lambda_{\mu_1} = \sum_{i=1}^C \lambda_i$. The test function F then simplifies to:

$$F(\mu_1(x_k)) = e^{-\lambda_{\mu_1} \cdot \min\{x_{k,1}, \dots, x_{k,C}\}}. \quad (3)$$

In practice, each λ_i is estimated as the reciprocal of the average activation value across the spatial dimension of the i^{th} channel in the feature map.

2. $\mu_2(X_k) = \sum_{i=1}^C X_{k,i}$ – Assuming that all λ_i are equal to λ_{μ_2} , the sum follows an Erlang distribution with shape parameter equal to the number of summed variables (C) and rate parameter equal to that of the common exponential distribution of parameters λ_{μ_2} , leading to:

$$F(\mu_2(x_k)) = \frac{\Gamma(C, \lambda_{\mu_2} \sum_{i=1}^C x_{k,i})}{\Gamma(C)}, \quad (4)$$

where $\Gamma(\cdot)$ and $\Gamma(\cdot, \cdot)$ are the Gamma and upper incomplete Gamma functions, respectively. Here, λ_{μ_2} is computed as

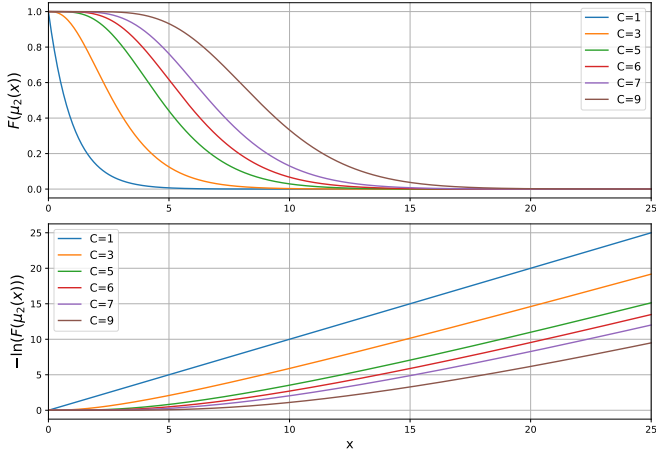


Figure 2: Variations of F_{μ_2} and $-\ln F_{\mu_2}$.

the reciprocal of the average activation value across all voxels in the feature map.

Our ablation study, detailed in Section 5, shows that the measure μ_2 (sensitive) outperforms μ_1 (conservative). This superiority may stem from a key limitation of μ_1 , which implicitly assumes that all channels must simultaneously exhibit target-like behavior, i.e. no channel i exhibits a background-like $x_{k,i}$ value, once one channel does. Such an assumption conflicts with the goal of extracting diverse and complementary features across the channels, potentially degrading the overall discriminative power of the representation. Consequently, we adopt μ_2 for the rest of the study. The shape of our test function is displayed in Figure 2. We report scores in terms of *significance* [23], i.e. $-\ln F(\mu(x_k))$, to enhance interpretability. To our knowledge, the use of an exponential hypothesis in this detection setting has not been previously explored. Its key advantage lies in its ability to explicitly push background activations towards zero, thereby simplifying the selection of detection thresholds under real-world conditions.

3.2. Integration within the YOLO framework

Architecture overview. The overall architecture is illustrated in Figure 3. The input image is first processed by a standard YOLO network, such as YOLOv7 or YOLOv9. To ensure the generality of our approach, we only modify the detection head of the YOLO network. Specifically, we decouple the prediction of the objectness scores from that of the bounding box coordinates and class scores. We then re-estimate the objectness score using our Anomaly-Aware Detection Head (AADH), which integrates the proposed statistical anomaly test. This process yields new objectness scores that range from 0 to 1, now reflecting the notion of anomaly with respect to the learned background distribution. The entire network, including the AADH, is trained end-to-end using the Mean Squared Error (MSE) loss for the objectness scores. We refer to the resulting architecture as **AA-YOLO** (Anomaly-Aware YOLO). When specifying the used backbone, e.g., YOLOv7, the network is called AA-YOLOv7.

Anomaly-Aware Detection Head. As illustrated in Figure 3, the AADH consists of three main components. First, a spatial filtering block is designed to capture and gather relevant spatial context around the central voxel of each predicted bounding box. This block includes two convolutional layers with a 3×3 kernel size, each followed by a Batch Normalization layer and ReLU activation. The output is a C -channel feature map, which then undergoes the statistical test $-\ln(F_{\mu_2})$ (where F_{μ_2} is given by Eq. (4)). The behavior of the function F_{μ_2} (cf. Figure 2) highlights that the choice of C influences the sharpness of F . Our ablation study suggests setting $C = 8$ for optimal detection performance. To ensure that the output scores from the statistical test fall between 0 and 1, we employ a scaled and zero-centered sigmoid activation function, parameterized by α , which effectively handles the asymmetry of the output scores. This activation function is defined as $\sigma_\alpha(x) = \frac{2}{1+e^{-\alpha x}} - 1$. Given that our statistical test produces scores that slowly increase (almost linearly, as shown in Figure 2) and reach particularly high values for targets, a smaller α (below 1) helps to stretch the sigmoid curve, allowing it to better capture the nuances of our output scores. Empirically, we find in our ablation study that setting $\alpha = 0.001$ leads to optimal performance, as it provides a suitable trade-off between sensitivity and specificity.

4. Experiments and results

4.1. Experimental set-up

Datasets. To evaluate our methods, we rely on two widely-adopted benchmarks for IRSTD: the SIRST dataset [8] and the IRSTD-1k dataset [24]. The SIRST dataset, one of the first publicly released real-image infrared small target datasets, is a commonly used reference in the literature. It consists of 427 mono-spectral infrared images with a resolution of 256×256 pixels. To assess our methods in frugal learning settings, we train on a subset of 25 images from the SIRST dataset, which represents less than 10% of the total dataset. To ensure the independence of our results from the training set, we randomly select three non-overlapping sets of 25 images and report the average results across these sets. In addition to SIRST, we also consider the challenging IRSTD-1k dataset, a recently published benchmark that provides a larger collection of 1000 images with a higher resolution of 512×512 pixels. Both datasets are divided into training, validation, and test sets with a ratio of 60 : 20 : 20, and we use the splits provided by [8] for SIRST and by [6] for IRSTD-1k. To meet the input size requirements of YOLO networks, all images are upscaled to 640×640 using bicubic interpolation.

Baselines. We evaluate our approach using several YOLO-based architectures with varying sizes, including YOLOv7 and lightweight versions such as YOLOv7-tiny (YOLOv7t) or YOLOv9-tiny (YOLOv9t). We also combine our approach with the loss and module proposed in [7]. We further explore the applicability of our method beyond detection by integrating AADH into a standard instance segmentation network, namely YOLOv5-seg. We compare our methods not only with standard YOLO baselines without AADH but also to advanced

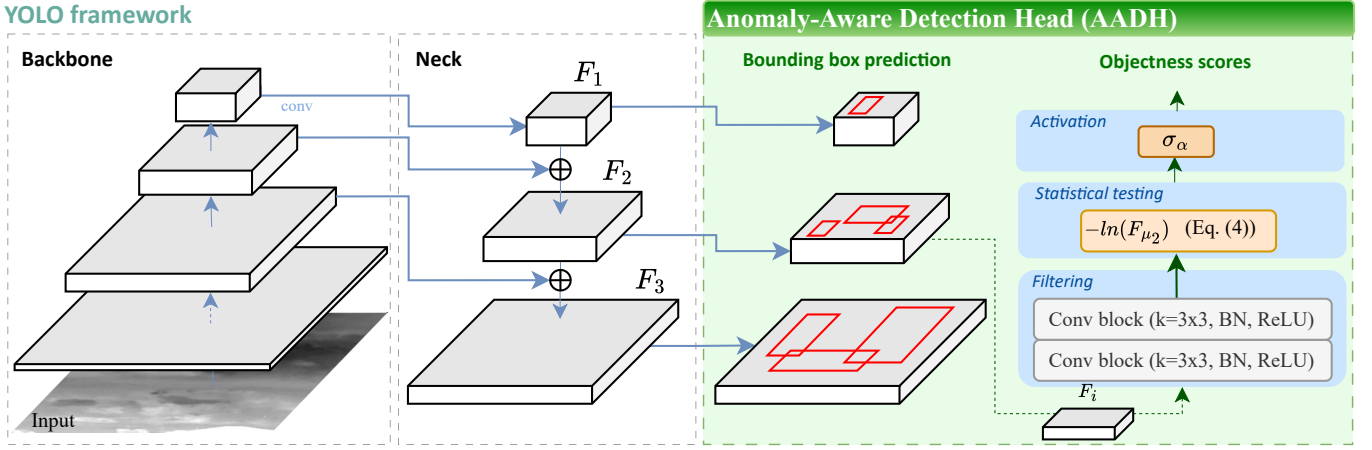


Figure 3: AA-YOLO architecture. The input first passes through a generic YOLO backbone to extract high-level features. Then, the conventional YOLO detection head is replaced by our Anomaly-Aware Detection Head (AADH), which enhances small object features by integrating statistical anomaly testing to estimate objectness scores. For simplicity, we illustrate the application of our AADH on F_2 -level feature maps only, although in practice AADH is applied to all detection scales: F_1 , F_2 and F_3 .

SOTA methods, including segmentation-based approaches like DNANet [1], AGPCNet [10], SCTransNet [2], SIRST-5K [25], MSHNet [12], DATransNet [3], and YOLO-based detectors like EFLNet [6] and YOLO+PConv+SD [7]. All YOLO baselines are trained from scratch using Nvidia V100 or A100 GPU for 600 epochs, with SGD optimizer and a batch size equal to 16. Additional training details for all methods are reported in the Appendix C. Note that our comparison focuses on SOTA deep learning-based methods for IRSTD, given that traditional approaches have been surpassed [1].

Evaluation metrics. Our evaluation relies on standard object-level metrics, namely the F1 score and the Average Precision (AP), i.e. the area under the precision-recall curve. To determine true positives, we adopt a relaxed criterion: a detected object is considered a true positive if its IoU with the ground truth is at least 5%. This low threshold is used to avoid penalizing results in cases where annotations are subjective, as presented in the Section 1. We also present the AP_s metric, which computes the AP for very small objects, i.e. those with a surface area of less than 5×5 pixels. We additionally report the IoU for instance segmentation methods, which can be compared to the SOTA segmentation IoU reported in the Appendix A. Finally, to gain a deeper understanding of the methods' sensitivity and detection capability, we provide their precision, recall, and false alarm rates per image in the Appendix A. Note that for segmentation methods, we convert the predicted segmentation maps to object-level predictions using the code provided by [1], which employs morphological operators.

4.2. New SOTA results on two IRSTD benchmarks

Quantitative results. Table 1 demonstrates that our AADH module consistently improves (with only rare exceptions) and uniformizes the object-level performance of various YOLO baselines on the SIRST and IRSTD-1k datasets, regardless of the encoder type, number of training parameters (provided in

Method	SIRST			IRSTD-1k		
	F1	AP	AP _s	F1	AP	AP _s
<i>SOTA</i>						
ACM	95.4	95.2	87.1	90.9	88.2	77.8
AGPCNet	93.8	92.2	93.0	91.1	88.9	74.1
DNANet	97.1	98.4	96.1	90.7	87.0	79.1
RDIAN	95.9	93.8	86.3	86.7	84.5	67.3
SCTransNet	95.4	95.9	92.9	91.9	90.8	87.0
SIRST-5K	96.8	98.1	95.2	90.1	89.3	86.7
MSHNet	94.8	95.6	92.3	92.0	91.1	88.8
DATransNet	93.5	92.3	74.9	89.1	86.7	73.2
EFLNet	96.9	98.3	97.6	92.5	96.5	89.8
YOLOv7 +PConv +SD	96.8	97.8	97.1	87.8	93.2	86.1
<i>YOLO baselines</i>						
YOLOv7	96.9	98.2	97.1	92.6	95.2	87.1
YOLOv7t	96.3	98.2	97.1	85.3	91.5	83.6
YOLOv9t	94.5	97.0	97.3	90.9	95.4	83.9
<i>Our methods - Object detection</i>						
AA-YOLOv7t +PConv +SD	96.9	98.0	97.0	91.1	96.0	89.5
AA-YOLOv7	97.9	<u>98.5</u>	98.0	91.2	95.6	86.3
AA-YOLOv7t	97.9	<u>98.5</u>	<u>97.9</u>	<u>92.5</u>	96.6	90.9
AA-YOLOv9t	<u>97.4</u>	98.6	97.8	91.4	95.8	87.9
<i>Instance segm.</i>						
YOLOv5-seg	95.8	98.2	56.5	87.6	91.9	34.8
AA-YOLOv5-seg	96.9	98.6	72.4	90.2	88.9	66.8

Table 1: Object-level results obtained on SIRST and IRSTD-1k datasets. Best results are in bold, and second best ones are underlined.

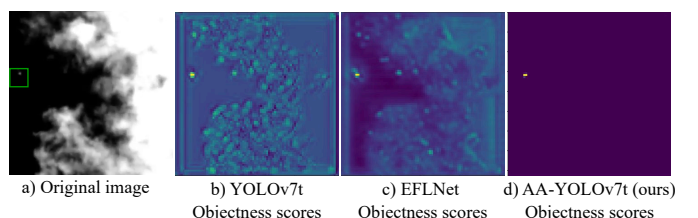


Figure 4: Objectness score maps for different methods.

Method	SIRST	IRSTD-1k
	IoU \uparrow	IoU \uparrow
<i>SOTA</i>		
ACM	63.5	60.3
AGPCNet	62.8	62.1
DNANet	65.3	62.1
RDIAN	64.1	61.3
SCTransNet	76.6	60.0
SIRST-5K	72.1	61.9
MSHNet	70.7	58.4
DATransNet	63.5	<u>62.4</u>
<i>YOLO-based instance segmentation</i>		
YOLOv5-seg	56.5	34.8
AA-YOLOv5-seg (ours)	<u>72.4</u>	66.8

Table 2: Pixel-level results obtained on SIRST and IRSTD-1k datasets. The best results are in bold, and the second best results are underlined.

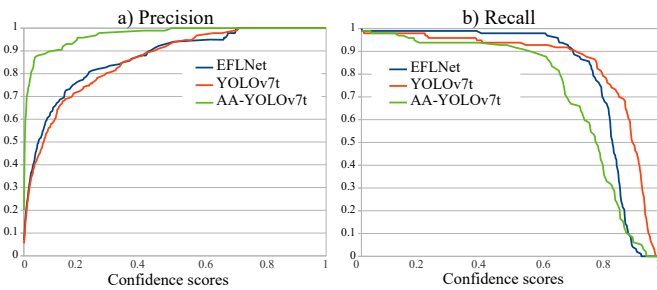


Figure 5: Precision and recall curves obtained on the SIRST dataset.

the Table 4), or initial performance levels. For instance, our smallest backbone YOLOv9t shows a 2.9% increase in F1 on the SIRST dataset and a 4.0% increase in AP_s on the IRSTD-1k dataset when integrating our AADH. Compared to SOTA methods, our approach i) outperforms segmentation-based methods, ii) benefits the method proposed by [7], and iii) is competitive with EFLNet. Notably, our best-performing configuration, AA-YOLOv7t, improves upon EFLNet by 1.1% in AP_s on IRSTD-1k while having six times fewer training parameters and a frugal design.

Last but not least, the results obtained with AA-YOLOv5-seg are particularly promising, as it performs competitively with SOTA segmentation methods on the SIRST dataset, achieving similar object and pixel-level metrics. Although it slightly underperforms the best segmentation methods on object-level metrics for IRSTD-1k, it significantly outperforms them in terms of IoU (with a margin of more than 4%, as shown in Table 2). It is worth noting that our AADH significantly enhances the pixel-level performance of YOLOv5-seg. This improvement can be attributed to the challenges posed by the IRSTD task, where YOLOv5-seg struggles to simultaneously learn segmentation and bounding box regression. Adding our statistical testing module helps to mitigate these challenges, resulting in a notable boost to the training process, as seen in the frugal setting. These findings suggest that our approach has the potential to improve instance segmentation methods for IRSTD, by combining object-level detection with fine-grained pixel-level

representation, which indicates a promising direction for future research.

Remark – The results presented in Table 2 for SOTA segmentation methods may slightly differ from the results reported in the original papers. This variation stems from our model selection approach, which differs from the original studies. Specifically, we select the best-performing model based on validation set performance, whereas the original papers often optimize on the test set. By decoupling model selection from test set performance, we aim to ensure a fair and unbiased evaluation process, thereby avoiding overfitting to the test set.

Qualitative analysis. Figure 4 shows that our method produces remarkably clean objectness score maps compared to YOLOv7t and EFLNet, with only small target scores emerging from a near-zero background. The optimization process is key to this behavior, as it enables the network to adjust feature representations in a way that: 1) targets are sufficiently distinct from the null hypothesis H_0 , allowing for accurate detection, and 2) background regions tend to conform to H_0 , mitigating the false alarms. This alignment, achieved through end-to-end training, is what makes our test operationally effective and robust: it allows for high precision rates, even at low detection thresholds, as confirmed by the precision curves provided in Figure 5. Crucially, this allows us to use a low, fixed threshold across all images, avoiding the need to manually tune it depending on image content or training conditions. This is a significant operational advantage over existing approaches, e.g. standard YOLO where the threshold often needs to be adjusted to prevent false alarms, as it enables us to set a robust default value with minimal risk of false alarms (since our method exhibits very few false alarms even at low thresholds).

4.3. Greater robustness in challenging conditions

Evaluating the robustness of a method is important to ensure its reliability, accuracy, and safety in real-world applications, where data are often imperfect, scarce, and uncertain. To further evaluate the benefits of AA-YOLO, we assess its robustness under various challenging conditions.

Few-shot training. Figure 6a presents the results obtained when the compared methods are trained on only 10% of the SIRST dataset (i.e., 25 images). All our AA-YOLO variants (represented by dark orange bars) achieve strong performance, close to those obtained with the full dataset. This robustness in frugal settings stems from our explicit use of background information to discriminate target pixels, which helps compensate for the lack of annotated data. In contrast, DNANet and EFLNet, although performing reasonably well, do not match the performance of our AA-YOLO variants, while YOLO baselines struggle even more.

Inference on noisy data. To evaluate robustness to noise, we add Gaussian noise with standard deviation $\sigma = 0.1$ to our test set. As shown in Figure 6b i), integrating AADH into YOLO baselines significantly increases their robustness to noisy inputs. Furthermore, our top-performing model, AA-YOLOv7t,

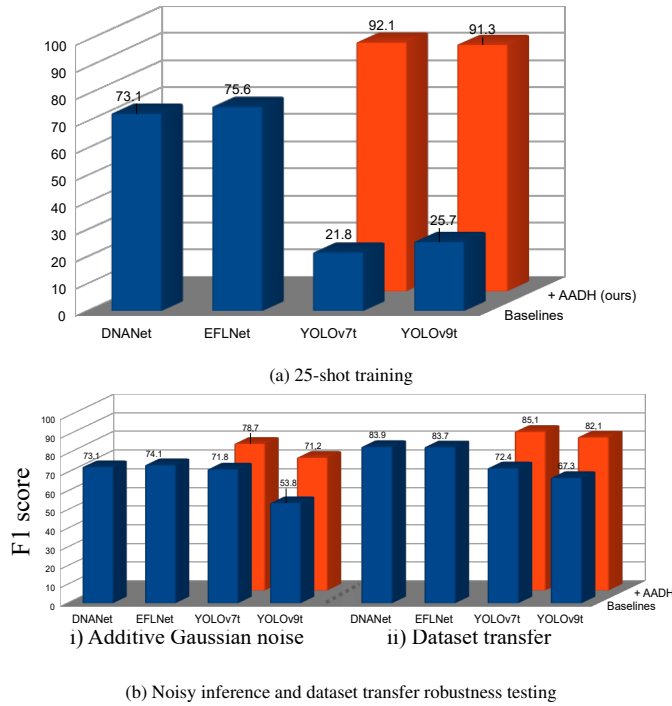


Figure 6: Robustness towards few-shot training, inference on noisy data and transfer learning.

outperforms EFLNet by over 4 points in F1 score, demonstrating superior robustness to noisy inputs. Figure 7 shows an example of inference on a particularly noisy data, with the absence of false alarms from our method highlighting the robustness of AADH in this context.

Transfer to another dataset. We also assess the transferability of detectors from the SIRST dataset to the more challenging IRSTD-1k dataset. Figure 6b ii) shows that our method enhances the performance of several YOLO baselines. For example, AADH improves YOLOv7t by 12.5 points, achieving a F1 score that is only 7.4 points below that obtained when directly trained on the IRSTD-1k dataset.

Transfer to another modality. Finally, we evaluate our algorithms in a real-world operational context using images captured with a mobile phone camera, which operates in the RGB modality and thus represents a different sensing scenario. The full-resolution images are presented in Appendix B; they depict a sky scene, with a drone visible in the first two images and absent in the last two. Figure 8 shows the detections produced by EFLNet and our best detector, AA-YOLOv7t, both set with a detection threshold of 0.1. Our method successfully detects the drone in the first two images with no false alarms. In contrast, EFLNet struggles to detect the drones and generates numerous false alarms. Although false alarms on trees may not be critical, the false alarm in the sky (last image) highlights EFLNet’s tendency to hallucinate targets. This shows the importance of assessing IRSTD algorithms on target-free scenes.

Statistical formulation	SIRST	
	F1	AP
$\mu_1 = \min\{X_1, \dots, X_C\}$	96.2	97.3
$\mu_2 = \sum_{i=1}^C X_i$	97.9	98.5
Gaussian background hypothesis	<u>97.6</u>	98.3
# Channels in AADH		
1	92.3	95.0
3	95.1	97.3
5	97.2	98.3
6	97.2	<u>98.4</u>
7	<u>97.6</u>	98.3
8	97.9	98.5
9	95.9	98.1
Activation function - α		
0.005	96.9	98.0
0.001	97.9	98.5
0.0005	97.1	<u>98.4</u>

Table 3: Ablation on the statistical testing formulation, using YOLOv7t backbone.

5. Ablation studies

This section provides the results of the ablation study performed on three components : 1) the formulation of the statistical test, 2) the number of channels in AADH, and 3) the parameter α in our activation function σ_α . We also provide the computational consumptions of our methods.

Statistical testing formulation. Table 3 compares three statistical formulations for AADH using the YOLOv7t backbone: the formulation using the μ_1 measure, the one using the μ_2 measure, and the Gaussian background hypothesis.

The comparison clearly shows that μ_2 significantly outperforms μ_1 : the F1 score improves by 1.7%. This superior performance can be attributed to the limitations of μ_1 , which assumes that all channels contain information about the target once one channel does. This assumption hinders the extraction of well-diversified features by the network, thereby reducing the quality of the extracted features. We also considered an alternative hypothesis, namely that the background follows a Gaussian distribution. Knowing that the sum of C independent standard normal random variables follows a χ^2 distribution with C degrees of freedom, the testing function evaluated on X_k boils down to $\frac{\Gamma(\frac{C}{2}, \frac{1}{2}\|X_k\|_2^2)}{\Gamma(C/2)}$. However, this assumption leads to slightly inferior detection performance, suggesting that the exponential assumption better aligns with the structure of the latent features.

Number of channels in AADH. Figure 2 illustrates the variations of F and $-\ln F$ for different values of C , where the choice of C influences the sharpness of F . We therefore perform an ablation study on the parameter C in the AADH using YOLOv7t backbone. The results presented in Table 3 show that very low values of C result in poor performance, while excessively high values (above 8) lead to training difficulties and make it harder

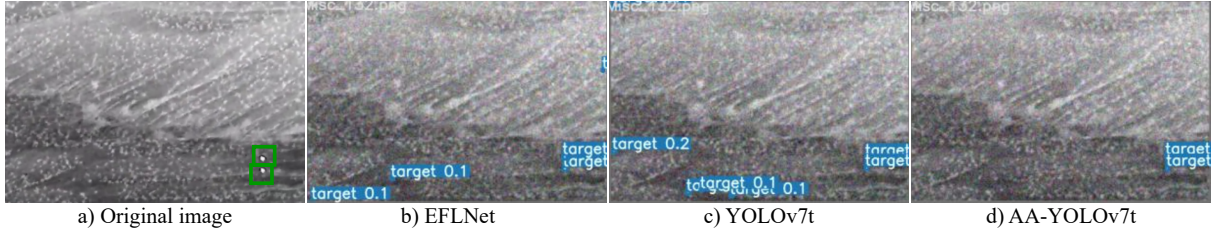


Figure 7: Detection results obtained on a particularly noisy image (with an additive Gaussian noise with spread $\sigma = 0.1$).



Figure 8: Results obtained in an operational context.

for the network to converge. To balance performance and stability, we recommend setting the number of channels C between 5 and 8, as this range avoids the aforementioned issues and ensures optimal results.

α parameter in σ_α activation function. The last three lines of Table 3 show that the choice of α has an impact on the performance. Specifically, setting $\alpha = 0.001$ leads to optimal performance when using AA-YOLOv7t.

Method	#P (M)↓	GFLOPs↓
DNANet	4.7	14.26
SCTransNet	11.2	20.24
EFLNet	38.3	102.2
YOLOv7+PConv+SD	6.0	14.0
AA-YOLOv7+PConv+SD	6.2	14.7
YOLOv5-seg	7.4	25.7
AA-YOLOv5-seg	7.6	26.3
YOLOv7	37.3	103.2
AA-YOLOv7	37.5	104.5
YOLOv7t	6.0	13.0
AA-YOLOv7t	6.2	13.7
YOLOv9t	1.4	5.0
AA-YOLOv9t	1.5	5.3

Table 4: Number of training parameters (#P, expressed in million (M)) and GFLOPs for the evaluated methods.

Computational consumption. Table 4 presents a computational analysis of our methods, including the number of model parameters and floating-point operations (FLOPs) expressed in GFLOPs. Our results show that adding the AADH module to the YOLO baseline incurs a negligible increase in parameters (approximately 0.2M) and FLOPs (around 5%). This suggests that our approach maintains the deployability of the baseline YOLO model while significantly improving performance and robustness under challenging conditions. Notably, our AA-YOLOv7t outperforms EFLNet, which has 6 times more parameters and 7 times more GFLOPs. Furthermore, when combined with a lighter backbone (such as YOLOv9t), our approach achieves comparable performance to EFLNet while using 25 times fewer parameters and 19 times fewer GFLOPs. This substantial reduction in computational cost makes our method an attractive solution for real-world applications.

5.1. Discussion about the versatility of our method

We have proposed a novel detection head, AADH, specifically designed for IRSTD. As demonstrated in the previous paragraphs, our method not only makes any YOLO-based model competitive with SOTA detectors, but also significantly enhances robustness under challenging conditions, thereby increasing its trustworthiness. The frugal nature of our contribution – a lightweight module added at the end of a YOLO network – enables seamless integration into various architectures and constraints.

Task versatility. A particularly noteworthy aspect of our approach is its versatility across tasks. Since our method relies solely on shape and pattern analysis, independent of the physical priors specific to IR imaging, it appears naturally suited to other tiny object detection tasks beyond IRSTD. For example, in remote sensing, detecting small objects such as vehicles in complex environments is a common challenge. This task differs from IRSTD by including a larger number of objects, some of which are larger and better resolved. It is therefore legitimate to question whether IRSTD methods can generalize effectively to such tasks. To address this question, we evaluated the effectiveness of our approach on the VEHicule Detection in Aerial Imagery dataset (VEDAI, [26]), which consists of 1200 IR satellite images with a resolution of 512×512 pixels. The results, presented in Table 5, show that YOLO baselines perform poorly on this task, despite their simplicity and operational appeal. In contrast, integrating our module into any YOLO detector, regardless of its size or complexity, yields highly competitive performance compared to EFLNet with significantly fewer

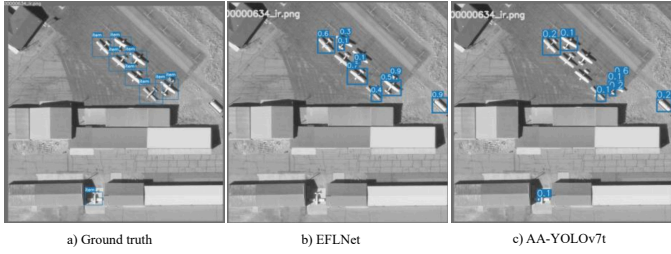


Figure 9: Illustration of the limits of our method on large, numerous vehicle detection. The image is extracted from the VEDAI dataset.

training parameters, while demonstrating robustness in various scenarios such as frugal setting. These findings suggest that our method can be confidently employed to achieve excellent performance in various small object detection tasks, particularly in settings with limited data or resources.

Architectural versatility. Our modular design provides architectural flexibility enabling us to address a wide range of challenges. By combining lightweight networks (e.g., YOLOv9t) with our AADH module, we can achieve high performance even in resource-constrained settings. Moreover, the modularity of our approach facilitates adaptation to different tasks, such as instance segmentation, which helps overcome common issues such as target adjacency and fragmentation. This results in accurate pixel-level predictions while maintaining object-level accuracy. Our design is also well-suited to scenarios involving architectural constraints. For example, when training conditions are very difficult, it is often beneficial to rely on pre-trained weights for the encoder to enhance the performance and robustness of the detectors. However, off-the-shelf pre-trained weights are only available for standard encoders such as ResNet50, ViT-B, or Swin Transformers. Unlike many IRSTD-specific methods in the literature that rely on custom encoders, we can easily add AADH to a YOLO with a generic encoder such as ResNet50 or Swin, and thus consider pre-trained weights. This advantage is particularly significant in light of recent advances in self-supervised learning, which have demonstrated considerable impact across vision tasks.

Limits and perspectives. While our method is well-suited for the detection of *unexpected* and rare events, it has limitations when it comes to detecting large and numerous objects. As shown in Figure 9, AA-YOLO tends to underdetect large and multiple planes in the VEDAI dataset compared to SOTA methods. This outcome is consistent with theoretical expectations: such objects no longer qualify as statistical anomalies with respect to the background and thus fall outside the scope of our anomaly-based detection strategy. While the statistical test relies on simplifying assumptions, it achieves robust performance in practice and avoids overfitting to spurious patterns, as shown by our ablations and transfer scenarios. More sophisticated probabilistic modeling is left as future work.

Method	#P (M)	VEDAI	
		F1	AP
EFLNet	38.3	<u>82.8</u>	87.2
YOLOv7	37.3	80.5	84.8
YOLOv7t	6.0	80.9	85.3
YOLOv9t	1.4	76.9	81.7
AA-YOLOv7	37.5	82.0	86.1
AA-YOLOv7t	6.2	83.0	<u>87.0</u>
AA-YOLOv9t	1.5	80.5	85.7

Table 5: Results obtained on the VEDAI dataset. #P is the number of training parameters, in million (M).

6. Conclusion

In this paper, we have presented AA-YOLO, a simple yet effective method to improve the detection of small targets in IR images. Our approach involves integrating a statistical anomaly testing directly into the detection head of YOLO-type networks, thereby enabling the detection of targets as deviation from the background distribution. Our method not only improves any YOLO detector for small object detection but also leads to SOTA results on two widely used IRSTD benchmarks. Last but not least, our AA-YOLO demonstrates a robustness that is all the more impressive in few-shot training (achieving 90% of the full-performance SIRST dataset), and the versatility of our approach allows it to adapt to various scenarios with severe resource constraints.

Acknowledgments – This project was provided with computing HPC and storage resources by GENCI at IDRIS thanks to the grant 2024-AD011015959 on the supercomputer Jean Zay’s V100 and A100 partitions.

References

- [1] B. Li, C. Xiao, L. Wang, Y. Wang, Z. Lin, M. Li, W. An, Y. Guo, Dense nested attention network for infrared small target detection, *IEEE Transactions on Image Processing* 32 (2022) 1745–1758.
- [2] S. Yuan, H. Qin, X. Yan, N. Akhtar, A. Mian, Sctransnet: Spatial-channel cross transformer network for infrared small target detection, *IEEE Transactions on Geoscience and Remote Sensing* 62 (2024) 1–15.
- [3] C. Hu, Y. Huang, K. Li, L. Zhang, C. Long, Y. Zhu, T. Pu, Z. Peng, Datransnet: dynamic attention transformer network for infrared small target detection, *IEEE Geoscience and Remote Sensing Letters* 22 (2025) 7001005.
- [4] J. Redmon, S. Divvala, R. Girshick, A. Farhadi, You only look once: Unified, real-time object detection, in: *Proceedings of the IEEE conference on computer vision and pattern recognition*, 2016, pp. 779–788.
- [5] G. Cheng, X. Yuan, X. Yao, K. Yan, Q. Zeng, X. Xie, J. Han, Towards large-scale small object detection: Survey and benchmarks, *IEEE Transactions on Pattern Analysis and Machine Intelligence* 45 (2023) 3333–3347.

ysis and Machine Intelligence 45 (11) (2023) 13467–13488.

[6] B. Yang, X. Zhang, J. Zhang, J. Luo, M. Zhou, Y. Pi, Eflnet: Enhancing feature learning network for infrared small target detection, *IEEE Transactions on Geoscience and Remote Sensing* 62 (2024) 1–11.

[7] J. Yang, S. Liu, J. Wu, X. Su, N. Hai, X. Huang, Pinwheel-shaped convolution and scale-based dynamic loss for infrared small target detection, in: *Proceedings of the AAAI Conference on Artificial Intelligence*, Vol. 39, 2025, pp. 9202–9210.

[8] Y. Dai, Y. Wu, F. Zhou, K. Barnard, Asymmetric contextual modulation for infrared small target detection, in: *Proceedings of the IEEE/CVF winter conference on applications of computer vision*, 2021, pp. 950–959.

[9] E. T. Jaynes, Information theory and statistical mechanics, *Physical review* 106 (4) (1957) 620.

[10] T. Zhang, L. Li, S. Cao, T. Pu, Z. Peng, Attention-guided pyramid context networks for detecting infrared small target under complex background, *IEEE Transactions on Aerospace and Electronic Systems* 59 (4) (2023) 4250–4261.

[11] H. Sun, J. Bai, F. Yang, X. Bai, Receptive-field and direction induced attention network for infrared dim small target detection with a large-scale dataset irdst, *IEEE Transactions on Geoscience and Remote Sensing* 61 (2023) 1–13.

[12] Q. Liu, R. Liu, B. Zheng, H. Wang, Y. Fu, Infrared small target detection with scale and location sensitivity, in: *Proceedings of the IEEE/CVF Conference on Computer Vision and Pattern Recognition*, 2024, pp. 17490–17499.

[13] C. Xu, J. Wang, W. Yang, H. Yu, L. Yu, G.-S. Xia, Rfla: Gaussian receptive field based label assignment for tiny object detection, in: *European conference on computer vision*, Springer, 2022, pp. 526–543.

[14] T. Ma, Z. Yang, Y.-F. Song, J. Liang, H. Wang, Dmef-net: Lightweight infrared dim small target detection network for limited samples, *IEEE Transactions on Geoscience and Remote Sensing* 61 (2023) 1–15.

[15] P. T. Nguyen, G. L. Nguyen, D. D. Bui, Lw-uav–yolov10: A lightweight model for small uav detection on infrared data based on yolov10, *Geomatica* (2025) 100049.

[16] L. Ruff, J. R. Kauffmann, R. A. Vandermeulen, G. Montavon, W. Samek, M. Kloft, T. G. Dietterich, K.-R. Müller, A unifying review of deep and shallow anomaly detection, *Proceedings of the IEEE* 109 (5) (2021) 756–795.

[17] P. Baldi, Autoencoders, unsupervised learning, and deep architectures, in: *Proceedings of ICML workshop on unsupervised and transfer learning*, JMLR Workshop and Conference Proceedings, 2012, pp. 37–49.

[18] H. H. Nguyen, C. N. Nguyen, X. T. Dao, Q. T. Duong, D. P. T. Kim, M.-T. Pham, Variational autoencoder for anomaly detection: A comparative study, *arXiv preprint arXiv:2408.13561* (2024).

[19] L. Ruff, R. Vandermeulen, N. Goernitz, L. Deecke, S. A. Siddiqui, A. Binder, E. Müller, M. Kloft, Deep One-Class Classification, in: *Proceedings of the 35th International Conference on Machine Learning*, PMLR, 2018, pp. 4393–4402. URL <https://proceedings.mlr.press/v80/ruff18a.html>

[20] H. Kwon, N. M. Nasrabadi, Kernel rx-algorithm: A non-linear anomaly detector for hyperspectral imagery, *IEEE transactions on Geoscience and Remote Sensing* 43 (2) (2005) 388–397.

[21] M. Shi, H. Wang, Infrared dim and small target detection based on denoising autoencoder network, *Mobile networks and applications* 25 (4) (2020) 1469–1483.

[22] H. Deng, Y. Zhang, Y. Li, K. Cheng, Z. Chen, Bemst: Multi-frame infrared small-dim target detection using probabilistic estimation of sequential backgrounds, *IEEE Transactions on Geoscience and Remote Sensing* 62 (2024) 5003815.

[23] S. L. Hégarat-Mascle, E. Aldea, J. Vandoni, Efficient evaluation of the number of false alarm criterion, *EURASIP J. Image Video Process.* (2019) 35.

[24] M. Zhang, R. Zhang, Y. Yang, H. Bai, J. Zhang, J. Guo, Isnet: Shape matters for infrared small target detection, in: *Proceedings of the IEEE/CVF Conference on Computer Vision and Pattern Recognition*, 2022, pp. 877–886.

[25] Y. Lu, Y. Lin, H. Wu, X. Xian, Y. Shi, L. Lin, Sirst-5k: Exploring massive negatives synthesis with self-supervised learning for robust infrared small target detection, *IEEE Transactions on Geoscience and Remote Sensing* 62 (2024) 1–11.

[26] S. Razakarivony, F. Jurie, Vehicle detection in aerial imagery: A small target detection benchmark, *Journal of Visual Communication and Image Representation* 34 (2016) 187–203.

Anomaly-Aware YOLO: A Frugal yet Robust Approach to Infrared Small Target Detection

Supplementary Materials

- YOLOv7 and YOLOv9-based methods were trained using the following repository: <https://github.com/WongKinYiu/yolov7>.
- (AA-)YOLOv5-seg networks were trained using the following repository: <https://github.com/ultralytics/yolov5>.

This document is the supplementary material of the paper entitled "Anomaly-Aware YOLO: A Frugal yet Robust Approach to Infrared Small Target Detection". It provides additional results and visualizations, as well as the details on the training parameters used for all methods.

Appendix A. Additional results and metrics

In order to gain a deeper understanding of the methods' sensitivity and detection capability, we provide their precision, recall, and false alarm rates per image on both SIRST and IRSTD-1k datasets in Table S1. Our findings show that our best method AA-YOLOv7t leads to the lowest false alarm rate. More specifically, on the SIRST dataset, AADH enhances precision, while on the IRSTD-1k dataset, it leads to a substantial increase in recall, which is a challenging metric for baseline methods. Importantly, this increase in recall comes at a very small cost to precision, showing that AADH demonstrates a good balance between precision and recall.

Appendix B. High-resolution operational data

Figure S1 displays the data used to evaluate the robustness of our algorithm under operational conditions, shown here in high resolution. Notably, the drone in the first image is nearly imperceptible to the naked eye, making it a challenging target to detect.

Appendix C. Training parameters

Table S2 provides the training configurations used for training SOTA segmentation networks, YOLO detectors and our methods on SIRST, IRSTD-1k and VEDAI datasets. The following sources were used for model training:

- EFLNet, SCTransNet, DATransNet, SIRST-5K and MSH-Net were trained using the original repository provided by the authors.
- For ACM, AGPCNet, and DNANet, we utilized the implementations and training parameters provided by DATransNet GitHub repository.

Backbone	AADH	SIRST						IRSTD-1k					
		F1↑	AP↑	P↑	R↑	Fa↓	AP _s ↑	F1↑	AP↑	P↑	R↑	Fa↓	AP _s ↑
ACM		95.4	95.2	95.6	95.2	0.07	87.1	90.9	88.2	92.7	89.2	0.11	77.8
AGPCNet		93.8	92.2	93.1	94.5	0.08	93.0	91.1	88.9	92.1	90.2	0.11	74.1
DNANet		97.1	98.4	96.9	97.3	0.04	96.1	90.7	87.0	90.6	90.9	0.14	79.1
RDIAN		95.9	93.8	93.9	98.2	0.08	86.3	86.7	84.5	88.7	84.8	0.16	67.3
SCTransNet		95.4	95.9	93.1	97.9	0.08	92.9	91.9	90.8	92.1	<u>91.7</u>	0.13	87.0
SIRST-5K		96.8	98.1	97.9	95.9	0.02	95.2	90.1	89.3	90.8	89.7	0.14	86.7
MSHNet		94.8	95.6	93.9	95.9	0.07	92.3	92.0	91.1	93.0	91.1	0.10	88.8
DATransNet		93.5	92.3	94.4	92.7	0.07	74.9	89.1	86.7	87.1	91.2	0.20	73.2
EFLNet		96.9	98.3	97.9	95.9	0.02	97.6	<u>92.5</u>	<u>96.5</u>	93.6	91.4	0.09	<u>89.8</u>
YOLOv7t +PConv+SD		96.8	97.8	<u>98.9</u>	94.8	<u>0.01</u>	97.1	87.8	93.2	92.7	83.4	0.10	86.1
YOLOv5-seg		95.8	98.2	96.8	94.8	0.04	97.6	87.6	91.9	90.1	85.1	0.14	83.7
YOLOv5-seg	✓	96.9	98.6	96.9	96.9	0.04	97.8	90.2	88.9	89.3	91.1	0.16	82.1
YOLOv7		96.9	98.2	96.0	<u>97.9</u>	0.05	97.1	92.6	95.2	93.0	92.3	0.10	87.1
YOLOv7	✓	97.9	98.5	97.9	<u>97.9</u>	0.02	98.0	91.2	95.6	93.1	89.4	0.09	86.3
YOLOv7t +PConv+SD		96.8	97.8	<u>98.9</u>	94.8	<u>0.01</u>	97.1	87.8	93.2	92.7	83.4	0.10	86.1
YOLOv7t +PConv+SD	✓	96.9	98.0	96.9	96.9	0.04	97.0	91.1	96.0	91.1	91.1	0.13	89.5
YOLOv9t		94.5	97.0	92.2	96.9	0.09	97.3	90.9	95.4	<u>94.0</u>	88.1	<u>0.08</u>	83.9
YOLOv9t	✓	97.4	98.6	<u>98.9</u>	95.9	<u>0.01</u>	97.8	91.4	95.8	<u>93.4</u>	89.4	0.09	87.9
YOLOv7t		96.3	98.2	<u>98.9</u>	93.8	<u>0.01</u>	97.1	85.3	91.5	84.4	86.1	0.24	83.6
YOLOv7t	✓	97.9	98.5	100.0	95.9	0.00	<u>97.9</u>	<u>92.5</u>	<u>96.6</u>	95.1	90.1	0.07	90.9

Table S1: Additional results and metrics obtained on SIRST and IRSTD-1k datasets. The best results are in bold, and the second best results are underlined.



Figure S1: High-resolution operational data. The first two images contain a drone that can be better seen in the zoomed-in view in the top-right corner, whereas the last two images are target-free.

Architecture	Parameter	Value
(AA-)YOLOv7, (AA-)YOLOv7t, (AA-)YOLOv5-seg, (AA-)YOLOv7t+PConv+SD	LR	0.01
	optimizer	SGD - weight decay: 0.0005
	scheduler	OneCycleLR - final LR: 0.1
	epochs	600
	batch size	16
(AA-)YOLOv9, (AA-)YOLOv9t	LR	0.01
	optimizer	SGD - weight decay: 0.0005
	scheduler	OneCycleLR - final LR: 0.01
	epochs	600
	batch size	16
EFLNet	LR	0.01
	optimizer	SGD - weight decay: 0.0005
	scheduler	OneCycleLR - final LR: 0.1
	epochs	600
	batch size	16
ACM, AGPCNet, DNANet, RDIAN, DATransNet	other	focal loss - gamma: 1.0
	LR	0.0005
	optimizer	Adam
	scheduler	MultiStepLR (steps: [200, 300], gamma: 0.1)
	epochs	400
SCTransNet	batch size	4
	LR	0.001
	optimizer	Adam
	scheduler	CosineAnnealingLR - η_{min} : 10^{-5}
	epochs	1000
SIRST-5K	batch size	4
	LR	0.05
	optimizer	Adagrad
	scheduler	CosineAnnealingLR - η_{min} : 10^{-5}
	epochs	1500
MSHNet	batch size	4
	LR	0.05
	optimizer	Adagrad
	scheduler	NA
	epochs	400
	batch size	4

Table S2: Training configurations used for SIRST, IRSTD-1k and VEDAI datasets.